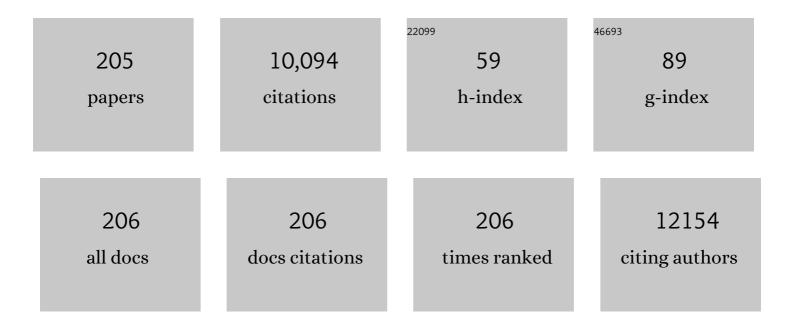
List of Publications by Year in descending order

Source: https://exaly.com/author-pdf/4747631/publications.pdf Version: 2024-02-01



#	Article	IF	CITATIONS
1	Bifunctional Auâ^'Fe <sub>3</sub> O <sub>4</sub> Heterostructures for Magnetically Recyclable Catalysis of Nitrophenol Reduction. Journal of Physical Chemistry C, 2011, 115, 6591-6598.	1.5	465
2	Characterization and distribution of polycyclic aromatic hydrocarbon contaminations in surface sediment and water from Gao-ping River, Taiwan. Water Research, 2004, 38, 1733-1744.	5.3	272
3	Solid-phase microextraction for determining the distribution of sixteen US Environmental Protection Agency polycyclic aromatic hydrocarbons in water samples. Journal of Chromatography A, 2000, 879, 177-188.	1.8	251
4	Stability of metal oxide nanoparticles in aqueous solutions. Water Science and Technology, 2010, 61, 127-133.	1.2	239
5	Composition and distribution of organochlorine pesticide residues in surface sediments from the Wu-Shi River estuary, Taiwan. Marine Pollution Bulletin, 2002, 45, 246-253.	2.3	197
6	Photocatalytic degradation of bisphenol A over a ZnFe2O4/TiO2 nanocomposite under visible light. Science of the Total Environment, 2019, 646, 745-756.	3.9	182
7	The influence of pH and cadmium sulfide on the photocatalytic degradation of 2-chlorophenol in titanium dioxide suspensions. Water Research, 2001, 35, 2873-2880.	5.3	179
8	Highly Sensitive and Selective Detection of Nanomolar Ferric Ions Using Dopamine Functionalized Graphene Quantum Dots. ACS Applied Materials & Interfaces, 2016, 8, 21002-21010.	4.0	168
9	Enhanced catalytic reduction of nitrophenols by sodium borohydride over highly recyclable Au@graphitic carbon nitride nanocomposites. Applied Catalysis B: Environmental, 2019, 240, 337-347.	10.8	153
10	Threeâ€Dimensional Hierarchically Ordered Porous Carbons with Partially Graphitic Nanostructures for Electrochemical Capacitive Energy Storage. ChemSusChem, 2012, 5, 563-571.	3.6	142
11	Determination of organochlorine pesticides and their metabolites in soil samples using headspace solid-phase microextraction. Journal of Chromatography A, 2001, 918, 177-188.	1.8	141
12	Characterization of Zr-Doped TiO2Nanocrystals Prepared by a Nonhydrolytic Solâ^'Gel Method at High Temperatures. Journal of Physical Chemistry B, 2006, 110, 20808-20814.	1.2	136
13	Highly sensitive and selective detection of mercury ions using N, S-codoped graphene quantum dots and its paper strip based sensing application in wastewater. Sensors and Actuators B: Chemical, 2017, 252, 1169-1178.	4.0	135
14	Simultaneous determination of pH, urea, acetylcholine and heavy metals using array-based enzymatic optical biosensor. Biosensors and Bioelectronics, 2005, 20, 1796-1804.	5.3	133
15	Highly efficient reduction of 4-nitrophenol by heterostructured gold-magnetite nanocatalysts. Applied Catalysis A: General, 2014, 486, 32-41.	2.2	122
16	Continuum-based models and concepts for the transport of nanoparticles in saturated porous media: A state-of-the-science review. Advances in Colloid and Interface Science, 2017, 246, 75-104.	7.0	119
17	N-Doped Graphene Quantum Dots-Decorated V <sub>2</sub> O <sub>5</sub> Nanosheet for Fluorescence Turn Off–On Detection of Cysteine. ACS Applied Materials & Interfaces, 2018, 10, 614-624.	4.0	117
18	Solubilization and mineralization of polycyclic aromatic hydrocarbons by Pseudomonas putida in the presence of surfactant. Journal of Hazardous Materials, 2003, 96, 15-27.	6.5	114

#	Article	IF	CITATIONS
19	Nano assembly of N-doped graphene quantum dots anchored Fe3O4/halloysite nanotubes for high performance supercapacitor. Electrochimica Acta, 2017, 245, 912-923.	2.6	111
20	Bipyridine- and Copper-Functionalized N-doped Carbon Dots for Fluorescence Turn Off–On Detection of Ciprofloxacin. ACS Applied Materials & Interfaces, 2020, 12, 32247-32258.	4.0	110
21	Photoassisted titanium dioxide mediated degradation of organophosphorus pesticides by hydrogen peroxide. Journal of Photochemistry and Photobiology A: Chemistry, 1997, 107, 239-244.	2.0	107
22	Immobilization and characterization of sol–gel-encapsulated acetylcholinesterase fiber-optic biosensor. Analytica Chimica Acta, 2001, 434, 239-246.	2.6	101
23	Cysteine-Mediated Reductive Dissolution of Poorly Crystalline Iron(III) Oxides by Geobacter sulfurreducens. Environmental Science & amp; Technology, 2002, 36, 2939-2945.	4.6	101
24	Dechlorination of tetrachloroethylene by palladized iron in the presence of humic acid. Water Research, 2005, 39, 2309-2318.	5.3	101
25	Dechlorination of trichloroethylene by Ni/Fe nanoparticles immobilized in PEG/PVDF and PEG/nylon 66 membranes. Water Research, 2009, 43, 3086-3094.	5.3	96
26	New Avenue for Appendage of Graphene Quantum Dots on Halloysite Nanotubes as Anode Materials for High Performance Supercapacitors. ACS Sustainable Chemistry and Engineering, 2017, 5, 4930-4940.	3.2	95
27	Visible-light photodegradation of sulfamethoxazole (SMX) over Ag-P-codoped g-C3N4 (Ag-P@UCN) photocatalyst in water. Chemical Engineering Journal, 2020, 384, 123383.	6.6	94
28	Surfactant enhanced remediation of cadmium contaminated soils. Water Science and Technology, 1998, 37, 65-71.	1.2	93
29	Determination of Distribution Coefficients of Priority Polycyclic Aromatic Hydrocarbons Using Solid-Phase Microextraction. Analytical Chemistry, 2000, 72, 3647-3652.	3.2	92
30	Characterization and composition of heavy metals and persistent organic pollutants in water and estuarine sediments from Gao-ping River, Taiwan. Marine Pollution Bulletin, 2008, 57, 846-857.	2.3	91
31	Graphene Quantum Dots Decorated Gold-Polyaniline Nanowire for Impedimetric Detection of Carcinoembryonic Antigen. Scientific Reports, 2019, 9, 7214.	1.6	91
32	Indirect Z-scheme nitrogen-doped carbon dot decorated Bi2MoO6/g-C3N4 photocatalyst for enhanced visible-light-driven degradation of ciprofloxacin. Chemical Engineering Journal, 2021, 422, 130103.	6.6	91
33	Interband Transitions in Solâ^'Gel-Derived ZrO <sub>2</sub> Films under Different Calcination Conditions. Chemistry of Materials, 2007, 19, 4804-4810.	3.2	90
34	Dual-template synthesis of magnetically-separable hierarchically-ordered porous carbons by catalytic graphitization. Carbon, 2011, 49, 3055-3064.	5.4	87
35	Ordered mesoporous carbon–TiO2 materials for improved electrochemical performance of lithium ion battery. Carbon, 2012, 50, 4259-4268.	5.4	86
36	The biomimic oxidase activity of layered V2O5 nanozyme for rapid and sensitive nanomolar detection of glutathione. Sensors and Actuators B: Chemical, 2018, 273, 1179-1186.	4.0	86

#	Article	IF	CITATIONS
37	Engineered Synthetic Polymer Nanoparticles as IgG Affinity Ligands. Journal of the American Chemical Society, 2012, 134, 15765-15772.	6.6	83
38	Activation of persulfate by CoO nanoparticles loaded on 3D mesoporous carbon nitride (CoO@meso-CN) for the degradation of methylene blue (MB). Science of the Total Environment, 2019, 675, 531-541.	3.9	83
39	Cu–TiO2 nanorods with enhanced ultraviolet- and visible-light photoactivity for bisphenol A degradation. Journal of Hazardous Materials, 2014, 277, 84-92.	6.5	81
40	Chemical-Composition-Dependent Metastability of Tetragonal ZrO2in Solâ^'Gel-Derived Films under Different Calcination Conditions. Chemistry of Materials, 2005, 17, 4837-4844.	3.2	79
41	Enhanced Dechlorination of Chlorinated Methanes and Ethenes by Chloride Green Rust in the Presence of Copper(II). Environmental Science & Technology, 2005, 39, 4082-4090.	4.6	79
42	Synergistic Effect of Copper Ion on the Reductive Dechlorination of Carbon Tetrachloride by Surface-Bound Fe(II) Associated with Goethite. Environmental Science & Technology, 2004, 38, 260-268.	4.6	78
43	Reductive Dechlorination of Carbon Tetrachloride and Tetrachloroethylene by Zerovalent Siliconâ~Iron Reductants. Environmental Science & Technology, 2003, 37, 2575-2581.	4.6	74
44	Enhanced photoactivity of Cu-deposited titanate nanotubes for removal of bisphenol A. Applied Catalysis B: Environmental, 2013, 129, 48-55.	10.8	71
45	Direct Synthesis of Controllable Microstructures of Thermally Stable and Ordered Mesoporous Crystalline Titanium Oxides and Carbide/Carbon Composites. Chemistry of Materials, 2010, 22, 1760-1767.	3.2	70
46	Sol–gel derived urease-based optical biosensor for the rapid determination of heavy metals. Analytica Chimica Acta, 2003, 481, 75-84.	2.6	69
47	Microwave-assisted hydrothermal synthesis of mesoporous anatase TiO2 via sol–gel process for dye-sensitized solar cells. Microporous and Mesoporous Materials, 2011, 142, 473-480.	2.2	68
48	Architectural design of hierarchically ordered porous carbons for high-rate electrochemical capacitors. Journal of Materials Chemistry A, 2013, 1, 2886.	5.2	68
49	Catalytic Nanoreactors of Au@Fe <sub>3</sub> O <sub>4</sub> Yolk–Shell Nanostructures with Various Au Sizes for Efficient Nitroarene Reduction. Journal of Physical Chemistry C, 2017, 121, 7844-7853.	1.5	68
50	Enhanced visible-light-responsive photodegradation of bisphenol A by Cu, N-codoped titanate nanotubes prepared by microwave-assisted hydrothermal method. Journal of Hazardous Materials, 2017, 322, 254-262.	6.5	67
51	Hierarchically Porous Carbon with Manganese Oxides as Highly Efficient Electrode for Asymmetric Supercapacitors. ChemSusChem, 2014, 7, 841-847.	3.6	65
52	Functionalized N-doped graphene quantum dots for electrochemical determination of cholesterol through host-guest inclusion. Mikrochimica Acta, 2018, 185, 526.	2.5	65
53	Visible-light photocatalytic diclofenac removal by tunable vanadium pentoxide/boron-doped graphitic carbon nitride composite. Chemical Engineering Journal, 2021, 403, 126213.	6.6	65
54	Preparation and characterization of urease-encapsulated biosensors in poly(vinyl alcohol)-modified silica sol–gel materials. Biosensors and Bioelectronics, 2007, 23, 66-73.	5.3	64

#	Article	IF	CITATIONS
55	The Effect of Chemical States of Dopants on the Microstructures and Band Gaps of Metal-Doped ZrO2Thin Films at Different Temperatures. Journal of Physical Chemistry B, 2004, 108, 18098-18103.	1.2	63
56	Photodegradation of parathion in aqueous titanium dioxide and zero valent iron solutions in the presence of hydrogen peroxide. Journal of Photochemistry and Photobiology A: Chemistry, 1998, 116, 221-228.	2.0	62
57	Solid-Phase Microextraction and Headspace Solid-Phase Microextraction for the Determination of High Molecular-Weight Polycyclic Aromatic Hydrocarbons in Water and Soil Samples. Journal of Chromatographic Science, 2000, 38, 528-534.	0.7	62
58	ZrO2 thin films with controllable morphology and thickness by spin-coated sol–gel method. Thin Solid Films, 2005, 489, 17-22.	0.8	62
59	Array-based titanium dioxide biosensors for ratiometric determination of glucose, glutamate and urea. Biosensors and Bioelectronics, 2010, 25, 1439-1446.	5.3	62
60	Coconut shell derived activated biochar–manganese dioxide nanocomposites for high performance capacitive deionization. Desalination, 2020, 492, 114602.	4.0	61
61	Sugarcane bagasse as the scaffold for mass production of hierarchically porous carbon monoliths by surface self-assembly. Microporous and Mesoporous Materials, 2012, 147, 47-52.	2.2	59
62	Hierarchically ordered mesoporous carbons and silver nanoparticles as asymmetric electrodes for highly efficient capacitive deionization. Desalination, 2016, 398, 171-179.	4.0	59
63	Electrically conducting graphene-based polyurethane nanocomposites for microwave shielding applications in the Ku band. Journal of Materials Science, 2017, 52, 1546-1560.	1.7	59
64	Multifunctional GQDs-Concanavalin A@Fe3O4 nanocomposites for cancer cells detection and targeted drug delivery. Analytica Chimica Acta, 2018, 1027, 109-120.	2.6	59
65	Heterostructured ZnFe <sub>2</sub> O <sub>4</sub> /TiO <sub>2</sub> nanocomposites with a highly recyclable visible-light-response for bisphenol A degradation. RSC Advances, 2017, 7, 50006-50016.	1.7	58
66	Boron-doped reduced graphene oxide-based bimetallic Ni/Fe nanohybrids for the rapid dechlorination of trichloroethylene. Environmental Science: Nano, 2017, 4, 565-576.	2.2	55
67	Reductive Dechlorination of Carbon Tetrachloride in Aqueous Solutions Containing Ferrous and Copper Ions. Environmental Science & Technology, 2004, 38, 6676-6684.	4.6	54
68	Femtomolar Detection of Dengue Virus DNA with Serotype Identification Ability. Analytical Chemistry, 2018, 90, 12464-12474.	3.2	54
69	Biomass–derived cellulose nanofibrils membrane from rice straw as sustainable separator for high performance supercapacitor. Industrial Crops and Products, 2021, 170, 113694.	2.5	54
70	Manipulating the morphology of 3D flower-like CoMn2O4 bimetallic catalyst for enhancing the activation of peroxymonosulfate toward the degradation of selected persistent pharmaceuticals in water. Chemical Engineering Journal, 2022, 436, 135244.	6.6	52
71	Fabrication of highly visible-light-responsive ZnFe <sub>2</sub> O <sub>4</sub> /TiO <sub>2</sub> heterostructures for the enhanced photocatalytic degradation of organic dyes. RSC Advances, 2016, 6, 103428-103437.	1.7	51
72	CoO-3D ordered mesoporous carbon nitride (CoO@mpgCN) composite as peroxymonosulfate activator for the degradation of sulfamethoxazole in water. Journal of Hazardous Materials, 2021, 401, 123326.	6.5	51

#	Article	IF	CITATIONS
73	One-Step Synthesis of Size-Tunable Gold@Sulfur-Doped Graphene Quantum Dot Nanocomposites for Highly Selective and Sensitive Detection of Nanomolar 4-Nitrophenol in Aqueous Solutions with Complex Matrix. ACS Applied Nano Materials, 2018, 1, 2153-2163.	2.4	50
74	Transformation of Carbon Tetrachloride by Thiol Reductants in the Presence of Quinone Compounds. Environmental Science & Technology, 2005, 39, 7460-7468.	4.6	49
75	Determination of organochlorine pesticide residues in foods using solid-phase extraction clean-up cartridges. Analyst, The, 1999, 124, 1287-1289.	1.7	48
76	Dual modality sensor using liposome-based signal amplification technique for ultrasensitive norovirus detection. Biosensors and Bioelectronics, 2020, 157, 112169.	5.3	48
77	Dechlorination of chlorinated hydrocarbons by bimetallic Ni/Fe immobilized on polyethylene glycol-grafted microfiltration membranes under anoxic conditions. Chemosphere, 2012, 86, 392-399.	4.2	47
78	Unveiling the hydrodechlorination of trichloroethylene by reduced graphene oxide supported bimetallic Fe/Ni nanoparticles. Chemical Engineering Journal, 2018, 334, 30-40.	6.6	46
79	Sensitive amperometric immunosensor for α-fetoprotein detection based on multifunctional dumbbell-like Au-Fe3O4 heterostructures. Sensors and Actuators B: Chemical, 2013, 186, 34-43.	4.0	45
80	Coupled removal of organic compounds and heavy metals by titanate/carbon nanotube composites. Water Science and Technology, 2008, 58, 1985-1992.	1.2	44
81	Few-Layered Phosphorene–Graphitic Carbon Nitride Nanoheterostructure as a Metal-Free Photocatalyst for Aerobic Oxidation of Benzyl Alcohol and Toluene. ACS Sustainable Chemistry and Engineering, 2020, 8, 13342-13351.	3.2	44
82	Activation of hierarchically ordered mesoporous carbons for enhanced capacitive deionization application. Synthetic Metals, 2015, 205, 48-57.	2.1	43
83	Sulfur-doped graphene quantum dot-based paper sensor for highly sensitive and selective detection of 4-nitrophenol in contaminated water and wastewater. RSC Advances, 2019, 9, 26588-26597.	1.7	43
84	Flower-like nickel hydroxide@tea leaf-derived biochar composite for high-performance supercapacitor application. Journal of Colloid and Interface Science, 2022, 623, 845-855.	5.0	43
85	Silver nanoparticles embedded boron-doped reduced graphene oxide as anode material for high performance lithium ion battery. Electrochimica Acta, 2017, 243, 282-290.	2.6	42
86	Nitrogen doped graphene quantum dot-decorated earth-abundant nanotubes for enhanced capacitive deionization. Environmental Science: Nano, 2020, 7, 228-237.	2.2	42
87	Glutamate optical biosensor based on the immobilization of glutamate dehydrogenase in titanium dioxide sol–gel matrix. Biosensors and Bioelectronics, 2006, 22, 185-191.	5.3	41
88	Industrial dye decolorizing lignin peroxidase from Kocuria rosea MTCC 1532. Annals of Microbiology, 2012, 62, 217-223.	1.1	40
89	One-pot biosynthesis of SnO2 quantum dots mediated by Clitoria ternatea flower extract for photocatalytic degradation of rhodamine B. Journal of Environmental Chemical Engineering, 2020, 8, 103879.	3.3	40
90	Dechlorination of Tetrachloroethylene in Aqueous Solutions Using Metal-Modified Zerovalent Silicon. Environmental Science & Technology, 2008, 42, 4752-4757.	4.6	38

#	Article	IF	CITATIONS
91	Enhanced photocatalytic degradation of sulfamethoxazole by visible-light-sensitive TiO2 with low Cu addition. Separation and Purification Technology, 2015, 156, 1003-1010.	3.9	38
92	Label-Free and Nondestructive Separation Technique for Isolation of Targeted DNA from DNA–Protein Mixture Using Magnetic Au–Fe <sub>3</sub> O <sub>4</sub> Nanoprobes. Analytical Chemistry, 2017, 89, 12244-12251.	3.2	38
93	Erbium-doped graphene quantum dots with up- and down-conversion luminescence for effective detection of ferric ions in water and human serum. Sensors and Actuators B: Chemical, 2021, 328, 129056.	4.0	37
94	Microstructural and photocatalytic properties of sol–gel-derived vanadium-doped mesoporous titanium dioxide nanoparticles. Journal of Non-Crystalline Solids, 2009, 355, 2302-2308.	1.5	36
95	A titanium dioxide/nitrogen-doped graphene quantum dot nanocomposite to mitigate cytotoxicity: synthesis, characterisation, and cell viability evaluation. RSC Advances, 2020, 10, 21795-21805.	1.7	36
96	Impedimetric biosensor for detection of cancer cells employing carbohydrate targeting ability of Concanavalin A. Biosensors and Bioelectronics, 2018, 122, 95-103.	5.3	35
97	Simultaneous determination of renal clinical analytes in serum using hydrolase- and oxidase-encapsulated optical array biosensors. Analytical Biochemistry, 2004, 334, 183-192.	1.1	34
98	Transformation of carbon tetrachloride by biogenic iron species in the presence of Geobacter sulfurreducens and electron shuttles. Journal of Hazardous Materials, 2009, 164, 337-344.	6.5	34
99	Synergistic effect of nickel ions on the coupled dechlorination of trichloroethylene and 2,4-dichlorophenol by Fe/TiO2 nanocomposites in the presence of UV light under anoxic conditions. Water Research, 2011, 45, 4198-4210.	5.3	34
100	Parameterization and prediction of nanoparticle transport in porous media: A reanalysis using artificial neural network. Water Resources Research, 2017, 53, 4564-4585.	1.7	34
101	Controlling distance, size and concentration of nanoconjugates for optimized LSPR based biosensors. Biosensors and Bioelectronics, 2020, 170, 112657.	5.3	34
102	Hollow magnetic-fluorescent nanoparticles for dual-modality virus detection. Biosensors and Bioelectronics, 2020, 170, 112680.	5.3	34
103	Boosting the energy storage performance of V <sub>2</sub> O <sub>5</sub> nanosheets by intercalating conductive graphene quantum dots. Nanoscale, 2020, 12, 16944-16955.	2.8	34
104	Insights into the rapid elimination of antibiotics from aqueous media by tunable C3N4 photocatalysts: Effects of dopant amount, co-existing ions and reactive oxygen species. Science of the Total Environment, 2019, 669, 1053-1061.	3.9	32
105	N-doping modified zeolitic imidazole Framework-67 (ZIF-67) for enhanced peroxymonosulfate activation to remove ciprofloxacin from aqueous solution. Separation and Purification Technology, 2022, 288, 120719.	3.9	32
106	Simultaneous determination of biomarkers for Alzheimer's disease using sol–gel-derived optical array biosensor. Biosensors and Bioelectronics, 2010, 25, 2464-2469.	5.3	31
107	Synthesis of Reduced Graphene Oxide/Titanium Dioxide Nanotubes (rGO/TNT) Composites as an Electrical Double Layer Capacitor. Nanomaterials, 2018, 8, 934.	1.9	31
108	Rapid removal of sulfamethoxazole from simulated water matrix by visible-light responsive iodine and potassium co-doped graphitic carbon nitride photocatalysts. Chemosphere, 2018, 210, 1099-1107.	4.2	31

#	Article	IF	CITATIONS
109	Dechlorination and photodegradation of trichloroethylene by Fe/TiO2 nanocomposites in the presence of nickel ions under anoxic conditions. Applied Catalysis B: Environmental, 2010, 100, 116-123.	10.8	30
110	Ternary Au/ZnO/rGO nanocomposites electrodes for high performance electrochemical storage devices. Applied Surface Science, 2017, 420, 118-128.	3.1	30
111	Application of sulfur-doped graphene quantum dots@gold-carbon nanosphere for electrical pulse-induced impedimetric detection of glioma cells. Biosensors and Bioelectronics, 2021, 181, 113151.	5.3	30
112	Coupled removal of bisphenol A and copper ion by titanate nanotubes fabricated at different calcination temperatures. Separation and Purification Technology, 2012, 91, 81-88.	3.9	28
113	Ultrasensitive Detection of the Hepatitis E Virus by Electrocatalytic Water Oxidation Using Pt-Co <sub>3</sub> O <sub>4</sub> Hollow Cages. ACS Applied Materials & Interfaces, 2020, 12, 50212-50221.	4.0	28
114	Nanoflower-like composites of ZnO/SiO2 synthesized using bamboo leaves ash as reusable photocatalyst. Arabian Journal of Chemistry, 2021, 14, 102973.	2.3	28
115	Enhanced dechlorination of carbon tetrachloride by Geobacter sulfurreducens in the presence of naturally occurring quinones and ferrihydrite. Chemosphere, 2014, 97, 54-63.	4.2	27
116	Enhanced photocatalytic activity of Cu-deposited N-TiO2/titanate nanotubes under UV and visible light irradiations. Separation and Purification Technology, 2017, 179, 403-411.	3.9	27
117	Self-assembled chromogen-loaded polymeric cocoon for respiratory virus detection. Nanoscale, 2021, 13, 388-396.	2.8	27
118	Electrochemically capacitive deionization of copper (II) using 3D hierarchically reduced graphene oxide architectures. Separation and Purification Technology, 2020, 251, 117368.	3.9	26
119	BSA-stabilized manganese phosphate nanoflower with enhanced nanozyme activity for highly sensitive and rapid detection of glutathione. Talanta, 2022, 237, 122957.	2.9	25
120	Characterization of interfacially electronic structures of gold–magnetite heterostructures using X-ray absorption spectroscopy. Journal of Colloid and Interface Science, 2014, 417, 325-332.	5.0	24
121	Synthesis and shielding properties of PVP-stabilized-AgNPs-based graphene nanohybrid in the Ku band. Synthetic Metals, 2016, 221, 86-94.	2.1	24
122	3-Dimensional ordered reduced graphene oxide embedded with N-doped graphene quantum dots for high performance supercapacitors. Electrochimica Acta, 2020, 361, 137018.	2.6	24
123	Fabrication of visible-light-driven tubular F, P-codoped graphitic carbon nitride for enhanced photocatalytic degradation of tetracycline. Journal of Environmental Chemical Engineering, 2022, 10, 106905.	3.3	24
124	Effect of substrate concentration on the biotransformation of carbon tetrachloride and 1,1,1-trichloroethane under anaerobic condition. Water Research, 1996, 30, 577-586.	5.3	23
125	Photoassisted reduction of metal ions and organic dye by titanium dioxide nanoparticles in aqueous solution under anoxic conditions. Science of the Total Environment, 2010, 408, 3334-3341.	3.9	23
126	Sustainable fabrication of green luminescent sulfur-doped graphene quantum dots for rapid visual detection of hemoglobin. Analytical Methods, 2019, 11, 4421-4430.	1.3	23

RUEY-AN DOONG

#	Article	IF	CITATIONS
127	Sustainable valorization of mesoporous aluminosilicate composite from display panel glasses waste for adsorption of heavy metal ions. Science of the Total Environment, 2019, 673, 337-346.	3.9	23
128	Ultrasensitive Detection of Tetracycline Using Boron and Nitrogen Co-Doped Graphene Quantum Dots from Natural Carbon Source as the Paper-Based Nanosensing Probe in Difference Matrices. Nanomaterials, 2020, 10, 1883.	1.9	23
129	Nitrogen and fluorine co-doped 3-dimensional reduced graphene oxide architectures as high-performance electrode material for capacitive deionization of copper ions. Separation and Purification Technology, 2021, 272, 117559.	3.9	23
130	Enhanced visible-light-driven photocatalytic degradation of acetaminophen over CeO2/I, K-codoped C3N4 heterojunction with tunable properties in simulated water matrix. Separation and Purification Technology, 2021, 272, 117567.	3.9	23
131	Photoâ€reduction and adsorption in aqueous Cr(VI) solution by titanium dioxide, carbon nanotubes and their composite. Journal of Chemical Technology and Biotechnology, 2011, 86, 949-956.	1.6	22
132	Fabrication of hierarchically ordered porous carbons using sugarcane bagasse as the scaffold for supercapacitor applications. Synthetic Metals, 2014, 194, 29-37.	2.1	22
133	Ultrafine CoO Embedded Reduced Graphene Oxide Nanocomposites: A High Rate Anode for Li–Ion Battery. ChemistrySelect, 2016, 1, 5758-5767.	0.7	22
134	Fluorescent and electrochemical dual-mode detection of Chikungunya virus E1 protein using fluorophore-embedded and redox probe-encapsulated liposomes. Mikrochimica Acta, 2020, 187, 674.	2.5	22
135	Microwave-assisted synthesis of SnO2/mesoporous carbon core-satellite microspheres as anode material for high-rate lithium ion batteries. Journal of Alloys and Compounds, 2019, 775, 214-224.	2.8	21
136	Synthesis and control of the morphology of SnO2 nanoparticles via various concentrations of Tinospora cordifolia stem extract and reduction methods. Arabian Journal of Chemistry, 2022, 15, 103738.	2.3	21
137	Size Effect of Ordered Mesoporous Carbon Nanospheres for Anodes in Li-Ion Battery. Nanomaterials, 2015, 5, 2348-2358.	1.9	20
138	Boron Doped Graphene Quantum Structure and MoS2 Nanohybrid as Anode Materials for Highly Reversible Lithium Storage. Frontiers in Chemistry, 2019, 7, 116.	1.8	20
139	A Z-scheme NiCo <sub>2</sub> O <sub>4</sub> /S codoped 1D g-C <sub>3</sub> N <sub>4</sub> heterojunction for solar-light-sensitive photocatalytic degradation of antibiotics in aqueous solutions exemplified by tetracycline. Environmental Science: Nano, 2022, 9, 229-242.	2.2	20
140	Clay-Supported Metal Oxide Nanoparticles in Catalytic Advanced Oxidation Processes: A Review. Nanomaterials, 2022, 12, 825.	1.9	20
141	Ultrasensitive detection of breast cancer cells with a lectin-based electrochemical sensor using N-doped graphene quantum dots as the sensing probe. Sensors and Actuators B: Chemical, 2022, 368, 132233.	4.0	20
142	Synergistic effect of Cu adsorption on the enhanced photocatalytic degradation of bisphenol A by TiO2/titanate nanotubes composites. Journal of the Taiwan Institute of Chemical Engineers, 2015, 57, 69-76.	2.7	19
143	Synthesis and characterization of Fe3O4/Polythiophene hybrid nanocomposites for electroanalytical application. Materials Chemistry and Physics, 2018, 205, 462-469.	2.0	18
144	Fe/Ni Bimetallic Organic Framework Deposited on TiO2 Nanotube Array for Enhancing Higher and Stable Photoelectrochemical Activity of Oxygen Evaluation Reaction. Nanomaterials, 2020, 10, 1688.	1.9	18

#	Article	IF	CITATIONS
145	Self-Assembled Chromogenic Polymeric Nanoparticle-Laden Nanocarrier as a Signal Carrier for Derivative Binary Responsive Virus Detection. ACS Applied Materials & Interfaces, 2021, 13, 36868-36879.	4.0	18
146	Fabrication and Characterization of Nanostructured Titanate Materials by the Hydrothermal Treatment Method. Recent Patents on Nanotechnology, 2008, 2, 84-102.	0.7	17
147	Adsorption and selective recognition of 17ß-estradiol by molecularly imprinted polymers. Journal of Polymer Research, 2012, 19, 1.	1.2	17
148	Plasmon Nanocomposite-Enhanced Optical and Electrochemical Signals for Sensitive Virus Detection. ACS Sensors, 2021, 6, 2605-2612.	4.0	17
149	A Review on Nanocellulose and Its Application in Supercapacitors. Macromolecular Materials and Engineering, 2021, 306, 2100556.	1.7	16
150	Characterization and photocatalytic activity of vanadium-doped titanium dioxide nanocatalysts. Water Science and Technology, 2009, 59, 523-530.	1.2	15
151	Size and morphological effect of Au–Fe3O4 heterostructures on magnetic resonance imaging. Journal of Nanoparticle Research, 2013, 15, 1.	0.8	15
152	Unveiling the thermal kinetics and scissoring mechanism of neolatry polyethylene/reduced graphite oxide nanocomposites. Journal of Analytical and Applied Pyrolysis, 2017, 123, 20-29.	2.6	15
153	PEC water splitting using mats of calcined TiO2 rutile nanorods photosensitized by a thin layer of Ni-benzene dicarboxylic acid MOF. Electrochimica Acta, 2021, 393, 139014.	2.6	14
154	Significance of Early and Late Stages of Coupled Aggregation and Sedimentation in the Fate of Nanoparticles: Measurement and Modeling. Environmental Science & Technology, 2018, 52, 8419-8428.	4.6	13
155	Nanomedicines Targeting Glioma Stem Cells. ACS Applied Materials & amp; Interfaces, 2023, 15, 158-181.	4.0	13
156	Enhanced Dechlorination of Tetrachloroethylene by Zerovalent Silicon in the Presence of Polyethylene Glycol under Anoxic Conditions. Environmental Science & Technology, 2011, 45, 2301-2307.	4.6	12
157	Enhanced dechlorination of tetrachloroethylene by polyethylene glycol-coated zerovalent silicon in the presence of nickel ions. Applied Catalysis B: Environmental, 2014, 144, 182-188.	10.8	12
158	Mesoporous silica supported bimetallic Pd/Fe for enhanced dechlorination of tetrachloroethylene. RSC Advances, 2015, 5, 90797-90805.	1.7	12
159	Biodegradable polyhydroxybutyrate/cellulose/calcium carbonate bioplastic composites prepared by heatâ€assisted solution casting method. Journal of Applied Polymer Science, 2022, 139, 51645.	1.3	12
160	Manganese ferrite decorated N-doped polyacrylonitrile-based carbon nanofiber for the enhanced capacitive deionization. Electrochimica Acta, 2022, 401, 139488.	2.6	12
161	Flower-like SnO2 Nanoparticle Biofabrication Using Pometia pinnata Leaf Extract and Study on Its Photocatalytic and Antibacterial Activities. Nanomaterials, 2021, 11, 3012.	1.9	12
162	Design of size-tunable molecularly imprinted polymer for selective adsorption of acetaminophen. Clean Technologies and Environmental Policy, 2017, 19, 243-250.	2.1	11

#	Article	IF	CITATIONS
163	Dual role of immunomodulation by crude polysaccharide from okra against carcinogenic liver injury in mice. Heliyon, 2021, 7, e06183.	1.4	11
164	Electrochemical immunosensor for ultra-sensitive detection of attomolar prostate specific antigen with sulfur-doped graphene quantum dot@gold nanostar as the probe. Electrochimica Acta, 2021, 389, 138700.	2.6	11
165	Formation of Cu <sub>2</sub> O/Titanate/Titania Heterojunctions from Hydrothermally Induced Dual Phase Transitions. Journal of Physical Chemistry C, 2016, 120, 21381-21389.	1.5	10
166	Ultra-small CoO nanocrystals anchored on reduced graphene oxide for enhanced lithium storage in lithium ion batteries. MRS Communications, 2017, 7, 236-244.	0.8	10
167	The photocatalytic degradation of methylene blue by green semiconductor films that is induced by irradiation by a light-emitting diode and visible light. Journal of the Air and Waste Management Association, 2018, 68, 29-38.	0.9	10
168	Effect of Lauric Acid on the Thermal and Mechanical Properties of Polyhydroxybutyrate (PHB)/Starch Composite Biofilms. International Journal of Polymer Science, 2020, 2020, 1-11.	1.2	10
169	Visible light sensitized porous clay heterostructure photocatalyst of zinc-silica modified montmorillonite by using tris(2,2′-bipyridyl) dichlororuthenium. Applied Clay Science, 2021, 204, 106023.	2.6	10
170	Effect of anionic and nonionic surfactants on sorption and micellar solubilization of monocyclic aromatic compounds. Water Science and Technology, 1996, 34, 327-334.	1.2	10
171	Comparative study on pilot-scale production of CuO-loaded activated biochar and hydrochar from oil-palm empty fruit bunches for high-performance symmetric supercapacitor application. Journal of Electroanalytical Chemistry, 2022, 905, 115970.	1.9	10
172	N-Doped Graphene Quantum Dots/Titanium Dioxide Nanocomposites: A Study of ROS-Forming Mechanisms, Cytotoxicity and Photodynamic Therapy. Biomedicines, 2022, 10, 421.	1.4	10
173	Recent Advances in Nanomaterialâ€based Optical Biosensors as Potential Pointâ€ofâ€Care Testing (PoCT) Probes in Carcinoembryonic Antigen Detection. Chemistry - an Asian Journal, 2022, 17, .	1.7	10
174	Enhanced biodegradation of carbon tetrachloride by the supplement of substrate and mineral ions under anaerobic condition. Water Environment Research, 1995, 67, 276-281.	1.3	9
175	Simultaneous Recovery of Display Panel Waste Glass and Wastewater Boron by Chemical Oxo-precipitation with Fluidized-Bed Heterogeneous Crystallization. ACS Omega, 2019, 4, 14057-14066.	1.6	9
176	Functionalized Fe/Ni@g-C <sub>3</sub> N <sub>4</sub> nanostructures for enhanced trichloroethylene dechlorination and successive oxygen reduction reaction activity. Environmental Science: Nano, 2020, 7, 3469-3481.	2.2	9
177	Highly efficient capacitive deionization of brackish water with manganese vanadate nanorod decorated reduced graphene oxide electrode. Environmental Science: Nano, 2021, 8, 2844-2854.	2.2	9
178	Recyclable Catalyst of ZnO/SiO2 Prepared from Salacca Leaves Ash for Sustainable Biodiesel Conversion. South African Journal of Chemical Engineering, 2022, 40, 134-143.	1.2	9
179	Comparison of a new mass-concentration, chain-reaction model with the population-balance model for early- and late-stage aggregation of shattered graphene oxide nanoparticles. Colloids and Surfaces A: Physicochemical and Engineering Aspects, 2019, 582, 123862.	2.3	8
180	Sustainable Desalination by 3:1 Reduced Graphene Oxide/Titanium Dioxide Nanotubes (rGO/TiONTs) Composite via Capacitive Deionization at Different Sodium Chloride Concentrations. Nanomaterials, 2019, 9, 1319.	1.9	8

#	Article	IF	CITATIONS
181	Cargo encapsulated hepatitis E virus-like particles for anti-HEV antibody detection. Biosensors and Bioelectronics, 2021, 185, 113261.	5.3	8
182	Influencing Factors in the Synthesis of Photoactive Nanocomposites of ZnO/SiO2-Porous Heterostructures from Montmorillonite and the Study for Methyl Violet Photodegradation. Nanomaterials, 2021, 11, 3427.	1.9	8
183	Electrical and Dielectric Properties of Exfoliated Thermally Reduced Graphene Based Polyurethane Nanocomposites. Journal of Nanoscience and Nanotechnology, 2017, 17, 8782-8790.	0.9	7
184	Aggregation and sedimentation of shattered graphene oxide nanoparticles in dynamic environments: a solid-body rotational approach. Environmental Science: Nano, 2018, 5, 1859-1872.	2.2	7
185	Water Photo-Electrooxidation Using Mats of TiO2 Nanorods, Surface Sensitized by a Metal–Organic Framework of Nickel and 1,2-Benzene Dicarboxylic Acid. Hydrogen, 2021, 2, 58-75.	1.7	7
186	MODELING TRANSPORT AND FATE OF CHLORINATED HYDROCARBONS GOVERNED BY BIOTIC TRANSFORMATION IN POROUS MEDIA. Water Research, 1998, 32, 39-46.	5.3	6
187	Preparation of Potassium Ferrate for the Degradation of Tetracycline. ACS Symposium Series, 2008, , 404-419.	0.5	6
188	Concentration effect of copper loading on the reductive dechlorination of tetrachloroethylene by zerovalent silicon. Water Science and Technology, 2010, 62, 28-35.	1.2	5
189	Fe <sub>3</sub> O <sub>4</sub> @SiO <sub>2</sub> nanoflakes synthesized using biogenic silica from <i>Salacca zalacca</i> leaf ash and the mechanistic insight into adsorption and photocatalytic wet peroxidation of dye. Green Processing and Synthesis, 2022, 11, 345-360.	1.3	5
190	Flower-like hierarchical Sn3O4/montmorillonite nanostructure for the enhanced microwave-induced degradation of rhodamine B. Advanced Powder Technology, 2022, 33, 103623.	2.0	5
191	Prospects of an engineered tumor-targeted nanotheranostic platform based on NIR-responsive upconversion nanoparticles. Materials Advances, 2021, 2, 7101-7117.	2.6	4
192	Effect of crude Ganoderma applanatum polysaccharides as a renoprotective agent against carbon tetrachloride-induced early kidney fibrosis in mice. Veterinary World, 0, , 1022-1030.	0.7	4
193	Enhanced Photocatalytic Activity of Zn-Al Layered Double Hydroxides for Methyl Violet and Peat Water Photooxidation. Nanomaterials, 2022, 12, 1650.	1.9	4
194	Erbium-Doped GQD-Embedded Coffee-Ground-Derived Porous Biochar for Highly Efficient Asymmetric Supercapacitor. Nanomaterials, 2022, 12, 1939.	1.9	4
195	Physicochemical properties of reduced graphite oxide conglomerated polyethylene nanocomposites. Polymer International, 2018, 67, 1638-1647.	1.6	3
196	Magnetically-separable photocatalyst of magnetic biochar from snake fruit peel for rhodamine B photooxidation. Environmental Nanotechnology, Monitoring and Management, 2022, 17, 100669.	1.7	3
197	Assessing the effect of calcination on adsorption capability of Mg/Al layer double hydroxides (LDHs). Materials Research Express, 2022, 9, 035505.	0.8	2
198	Magnetically Recyclable Goldâ^'Magnetite Nanocatalysts for Reduction of Nitrophenols. ACS Symposium Series, 2013, , 291-305.	0.5	1

#	Article	IF	CITATIONS
199	Application of Zerovalent Silicon for the Dechlorination of Chlorinated Hydrocarbons – A Review. ACS Symposium Series, 2013, , 211-231.	0.5	1
200	Reply to Comment on "Chemical-Composition-Dependent Metastability of Tetragonal ZrO2 in Sol–Gel-Derived Films under Different Calcination Conditions― Chemistry of Materials, 2012, 24, 4270-4270.	3.2	0
201	Fabrication of Titanium Dioxide Nanotube Array as a Photocathode for Hydrogen Evolution. ACS Symposium Series, 2014, , 133-147.	0.5	Ο
202	Effect of Mesoporous Nanoparticles from LCD Glass Panels Waste toward Polypropylene Based Hybrid Composites. , 2018, , .		0
203	Cover Image, Volume 67, Issue 12. Polymer International, 2018, 67, i-i.	1.6	0
204	Immunomodulating effect of Polysaccharide Krestin from cariolus versicolor grown in Indonesia against Rheumatoid arthritis in rat. Research Journal of Pharmacy and Technology, 2021, 14, 1360-1364.	0.2	0
205	Synthesis and Study of the Photodynamic Activity of Titanium-based Nanocomposites on MDA-MB-231 Cells. , 2020, , .		Ο